In-Situ Failure Identification in Woven Composites throughout Impact using Fiber Bragg Grating Sensors

James Pearson, Mohanraj Prabhugoud, Mohammed Zikry, Kara Peters[1]

North Carolina State University, Department of Mechanical and Aerospace Engineering, Campus Box 7910, Raleigh, NC 27695, Tel: 1.919.515.5226, Fax: 1.919.515.7968

ABSTRACT

In this study, measurements from low-impact velocity experiments and surface mounted optical fiber Bragg grating (FBG) sensors were used to obtain detailed information pertaining to damage progression in two-dimensional laminate woven composites. The woven composites were subjected to multiple strikes at 2m/s until perforation occurred, and the impactor position and acceleration were monitored throughout each event. From these measurements, we obtained dissipated energies and contact forces. The FBG sensors were surface mounted at different critical locations near penetration-induced damaged regions. These FBG sensors were used to obtain initial residual strains and axial and transverse strains that correspond to matrix cracking and delamination. The transmission and the reflection spectra were continuously monitored throughout the loading cycles. They were used, in combination with the peak contact forces, to delineate repeatable sensor responses corresponding to material failure. From the FBG spectra, fiber and matrix damage were separated by an analysis based on the behavior of individual Bragg peaks as a function of evolving and repeated impact loads. This provided an independent feedback on the integrity of the Bragg gratings. Thus, potential sources of error such as sensor debonding were eliminated from the strain data throughout the measurements. A comparison by number of impact strikes and dissipated energies corresponding to material perforation indicates that these measurements can provide accurate failure strains.

Keywords: Composite failure, fiber-optic Bragg sensor, residual strains, low-velocity impact

1. INTRODUCTION

Composites are being extensively used in military[1], commercial aerospace[2] and automotive[3] industries as well as bridge[4] and ship[5] construction. FBG sensors are being used in conjunction with composites to monitor and measure local strains at critical structural locations. These composites are highly susceptible to instantaneous failure because failure modes can initiate at the subsurface, and hence it is not easily detetacble.[6]

The development of low-loss, high-quality optical fiber for the telecommunications industry in the 1970's has spurred the extensive use of optical fiber Bragg grating (FBG) sensors for the measurement of failure strains in the aerospace and textile industries, with in flight testing scheduled for commercial airliners[7,8] and the X38/CRV spacecraft[9]. Particular attention has been devoted to the application of FBG sensors for monitoring the behavior of fiber reinforced composites during fabrication[10-13] and in-use service[4,14-16] due to the sensor's unique advantages over conventional foil strain gauges such as accurate local strain measurements, high resolution and signal bandwidth[17], small size, light weight[18], single-fiber multiple-gauge multiplexing ability[4,18] and the ability to withstand high heat and pressure with long term stability[17].

However, one of the major challenges in using these sensors for low-velocity impact, is to be able to relate local measured strains, which would be obtained in terms of bandwidth and Bragg wavelength shift to overall damage initiation and progression in the composite. Furthermore, material damage must be clearly delineated from optical fiber damage, hence material interactions between a host material and an embedded or mounted sensor must be characterized and the placement of sensors at critical locations must be identified a priori.

In this paper, we investigate how damage initiates and evolves at critical locations in laminated 2D woven composite panels that are subjected to low-velocity impact. FBG sensors are both surface mounted and embedded before impact,

[1] kjpeters@eos.ncsu.edu; phone 1 919 515 5226; fax 1 919 515 7968

and the overall mechanical response is combined with local strain measurements and damage characterization to obtain a detailed understanding of how failure evolves at different scales. Based on these measurements, our results indicate that the contact force, as a function of the measured local strain, can be classified into five regimes which correspond to the damage progression of the 2D woven laminated composites. These regimes can provide a guide to determining the local level of damage at critical locations for heterogeneous materials subjected to impact loading conditions. The paper is organized as follows: In Section 2, the experimental setup for mounting, impacting and interrogating the sensors is described, in Section 3 the results for the impact tests and strain measurements separated by method of sensor application are presented, and in Section 4 the conclusions are summarized.

2. EXPERIMENTAL METHODS AND MEASUREMENTS

An instrumented drop tower was used to impact the two-dimensional woven composites at low velocities and optical FBGs were used. The strains were obtained by a laser interrogation system from the FBG spectrum.

2.1 Material Preparation and Sensor Positioning

Composite specimens were fabricated from a twill woven carbon fiber prepreg with thermoset epoxy matrix as seen in Figure 1. All specimens were approximately 4.16 mm thick and consisted of 24 stacked prepreg lamina squares mutually aligned in the weave direction, and they were consolidated in a 12.7 cm square aluminum mold at 80° C and 180 psi for 3 hours with an additional 30 minutes of pressure during cool down.

MBond 200 strain gauge adhesive was used for surface mounting the FBGs on two separate composite specimens, which will be referred to as C1 and C2. Before use, the optical fiber's polyimide coating in the vicinity of the Bragg grating gauge was chemically stripped with acetone to increase the sensitivity and transfer of strain to the sensitive fiber core region[16,19]. After aligning the fibers with the direction of the top lamina's weave, the optical fiber was tensioned slightly to be straight, and it was adhered to the rear face of the composite specimen approximately 1.43 cm from the chosen point of impact on the front face.

A single FBG was embedded for specimen C3 with the optical fiber positioned at the center of the mid plane and aligned with the weave direction similar to C1 and C2. The fabrication of C3 was different from C1 and C2 to allow for embedding, and it was performed in three stages. In the first stages two 11-layer panels were prefabricated with the mold, and in the final stage an FBG was oriented between two fresh square prepreg laminas and this arrangement then sandwiched between both 11-layer panels sans mold before final pressing. This technique made use of the thermoset polymer's integrity under additional heating in the third stage to retain the 12.7 cm square shape.

2.2 Instrumented Drop Tower for Low-Velocity Impact

The instrumented drop tower consists of a 19 mm diameter hemispherical hardened steel indentor mounted to an adjustable 5.5 kg aluminum crosshead capable of delivering between 1-500 Joule impacts. All impacts were conducted at 2 m/s and a nominal incident kinetic energy of 11 Joules. Specimens were securely clamped and supported from underneath on a three inch steel ring with a thin neoprene mat on the surface to protect the optical fiber at rough edges and transitions. Specimens C3 and C2 were tested with the impactor's line of action aligned through the center of the support ring. Specimen C1 was tested differently with a support ring eccentric to the impactor thus effecting an apparent increase in support and number of strikes to penetration by bringing the point of impact and steel support ring closer.

The experiment was stopped when complete perforation of the composite panel occurred. Using an oscilloscope, contact force and dissipated energy for each strike were obtained through both the crosshead's acceleration during impact and the entry and exit velocities of the impactor. Contact force data was filtered using a 0.46 millisecond moving average to remove the characteristic oscillations in contact force with damage growth[20-22] during impact.

2.3 Data acquisition systems

FBG interrogation was carried out after each strike using a Tunics tunable laser unit using a scan step size of 0.01 nm, corresponding to a strain resolution of 4.4 $\mu\varepsilon$ at a Bragg wavelength of 1500 nm. Initially, prior to damage progression in the sensor, the strain was calculated from the Bragg peak shift of the FBG through,

$$\varepsilon_{Axial} = \frac{\Delta\lambda_B}{\lambda_B(1-p_e)} \tag{1}$$

where the photoelastic constant of the sensors was calibrated to be p_e = 0.22. The interpretation of the strain field once damage occurred in the sensor is discussed later in the experimental results section. A photodetector was used to convert the optical signal from the FBG into an analog signal. LabView software was used as the data acquisition system, and the measured spectrum in terms of transmission intensity and wavelength was stored for each impact event. The time required to complete one interrogation of the FBG was determined by the speed of tuning the laser through the scan range at the input incremental step size. This was approximately 15 seconds, thus precluding obtaining strain measurements where the total signal time length, measured as the contact duration between impactor and specimen, was greater than approximately 10 ms.

For specimen C1, instead of saving strain measurements as FBG spectrums through LabView, a Micron Optics Si720 spectrum analyzer was used to continuously probe the strain gauge at 5 Hz frequency. Displayed spectra were recorded in real time via digital video, which was later converted to still frames before being digitized into terms of intensity and wavelength as with specimens C3 and C2. This method lowered the strain resolution to approximately 90 με at 1500 nm.

3. RESULTS AND DISCUSSION

3.1 Surface mounted FBG

Specimens C1 (eccentrically impacted) and C2 (centered impacts) are shown with surface mounted gauges after penetration in Figure 1. As seen from this figure, the gauge was oriented so that axial strains in the optical fiber were recorded in the direction of the prepreg weave. Under impact, sample C1 required 105 strikes and sample C2 required 20 strikes for complete penetration. Despite the difference in number of strikes, which was due to an eccentric support and impactor for C1, the total dissipated energy in puncturing both panels was approximately the same. Specimen C1 had a dissipated energy of 112.9 Joules, and specimen C2 had a dissipated energy of 139.3. These values compare very well to the average dissipated energy calculated for puncturing a batch of identical composite samples at 139.4 Joules.

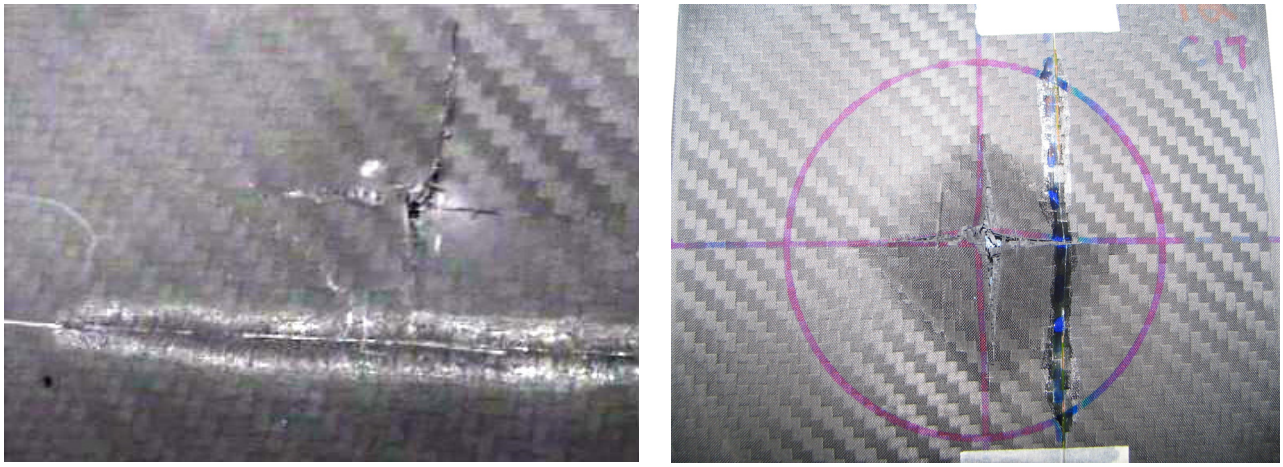

(a) **(b)**

Figure 1: Perforated composite panels (a) C1 and (b) C2 at the conclusion of the experiment. The 8 mm long gauge length of the FBG is centered in the optical fiber along the horizontal line in (b) with similar location in (a). Adhesive and localized fiber debonding and fracture occurred near the point of impact prior to full penetration of the specimen.

Surface mounted FBGs fractured well before complete penetration of the composite. For specimen C1, this occurred during strike 82, and for specimen C2 this occurred during strike 11 at which point both specimens had localized

debonding near the impact point. After the optical fiber initially fractured, strain interrogation was still possible from the FBGs by probing the Bragg wavelength in reflection mode instead of transmission mode.

Prior to fiber fracture and surface debonding however, post impact strains measurement by the FBGs were obtained, as seen in Figure 2. Sensor response can be classified into five regimes based on the Bragg peak wavelength shift and spectrum shape. The regimes and their characteristics are displayed in Table 1.

Table 1: FBG sensor response and strain interpretation for all five identified regimes.

Deformation Regime	Strain Response	FBG Signal Response
1	Gradual increase in axial tension	Bragg peak shift with uniform bandwidth
2	Increase in non-uniformity of axial tension	Spectrum bandwidth increase Tensile shift in Bragg peak
3	Maximum axial tension	Maximum Bragg peak shift
4	Axial strain decreases into compression	Bragg peak shift into compression
5	Uniform compressive axial strain fluctuations	Fluctuating peak shift Small drop in bandwidth

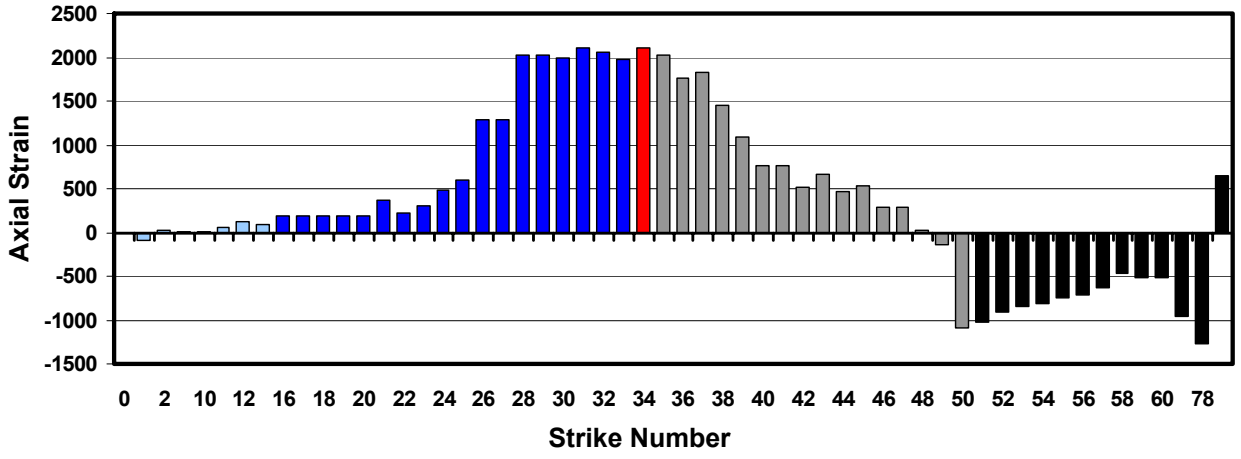

(a)

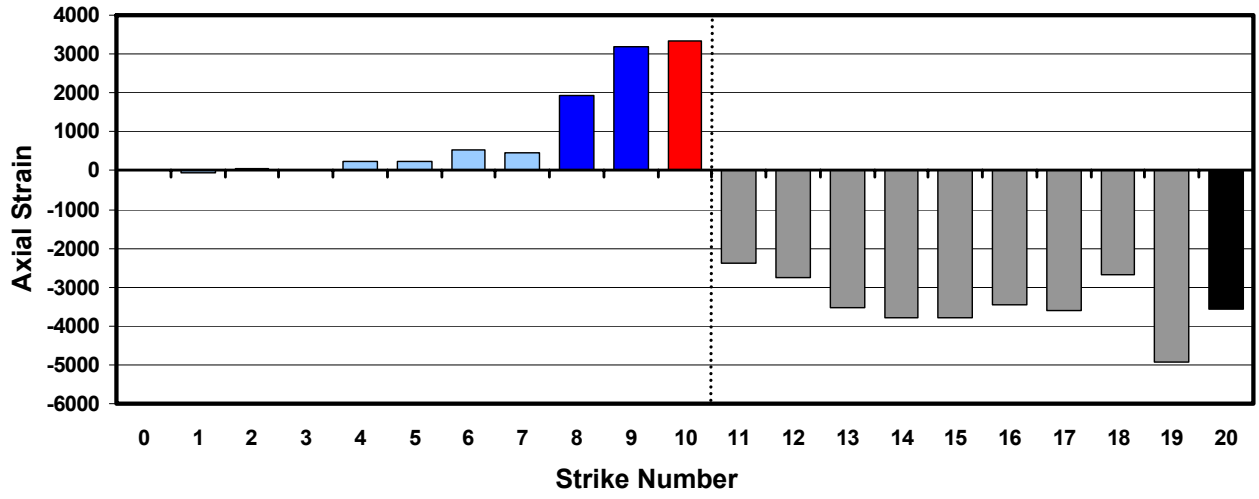

(b)

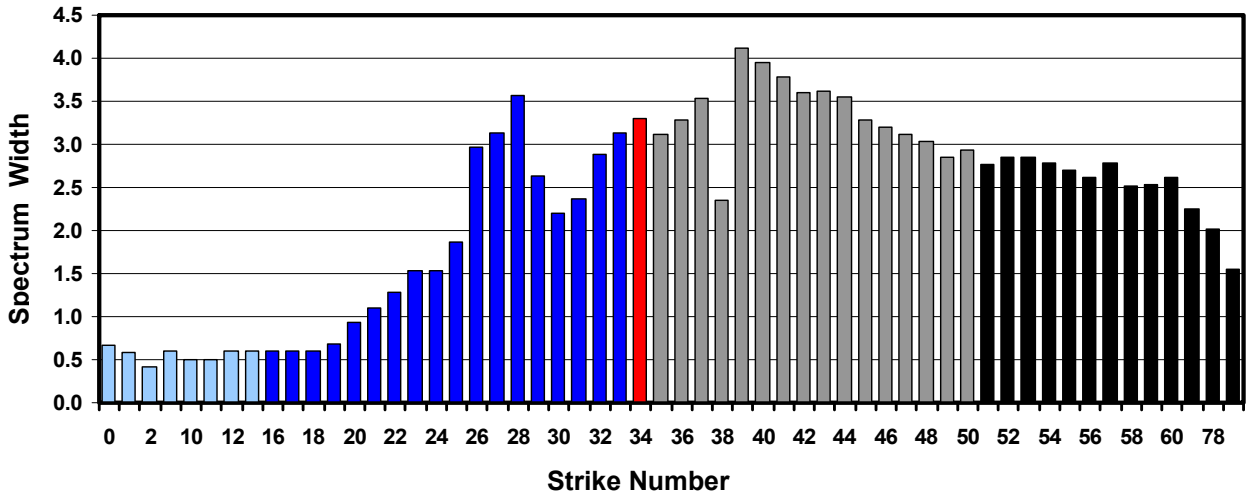

(c)

Figure 2: Post impact residual strain (in με) measured with surface mounted FBG after each impact for (a) C1 and (b) C2. Regimes are indicated by color with light blue regime 1, dark blue regime 2, red regime 3, gray regime 4 and black regime 5. For specimen C2 in (b), where multiple strain values are recorded after each strike, only the single largest magnitude strain is plotted. Optical fiber fracture denoted with dotted vertical line in (b). Specimen C1 FBG spectrum width (in nm), indicating non-uniformity of axial strain as opposed to simply axial strain as in (a) & (b), shown in (c). Strikes not shown have measurements similar to closest displayed neighboring strike.

Regimes 4 and 5, shown in gray and black in Figure 2, are where the predominant debonding and optical fiber fracture occurred, hence these measurements relate to the optical fiber failure and not to the local composite strains.

Video analysis of the continuous post impact probing of specimen C1 revealed a time dependence of the residual impact strains. Measurable relaxation of tensile strains in the tens of seconds immediately following impact indicated an additional form of storing and dissipating impact energy though internal friction between delaminated plies. A relaxation of strain occurred both in axial shifts and in the spectrum bandwidth of axial strains in each regime. Table 2 displays one selected strike from each regime broken down by both *relaxation type* and effective total axial strain decrease. In regime 5 the strain appears to increase when it should be relaxing because of the competing effect between decreasing spectra width and tensile Bragg peak center shift.

Table 2: Post impact tensile strain relaxation by regime for composite C1. All strain in με, Bragg peak shift and spectrum width change in nm, length of relaxation time monitored after impact measured in seconds. Note the two forms of possible relaxation, uniform Bragg peak center shift and Bragg spectrum bandwidth change.

Regime	Strike #	Elapsed Relaxation Time	Center Shift	Δε *Relaxation*	Bandwidth Change
1	12	15	-0.07	***-61***	0
2	25	40	-0.1	***-87***	-0.769
3	34	25	-0.6	***-521***	-1.2
4	44	15	0	***0***	-1.25
5	66	20	0.58	***503***	-0.833

We also correlated the global contact force data with local strain measurements and optical microscopy images of the damage progression, which indicated a characteristic failure path for all the surface mounted FBGs. In Figure 3, a plot of the peak contact force at measured residual impact strain for all strikes of Specimen C2 is shown. For each regime one strike was selected and an image of the visible surface damage shown.

As seen, the contact force decreases and both contact duration and dissipated energy or damage degree[21] increase with additional numbers of strikes and impact damage, which indicates a strength degradation of the material[1]. This is seen clearly in regimes 1 through 3 by the decreasing peak force and the increasing axial strain circuit traced out in Figure 3. Surface strains from regimes 4 and 5 in the bottom of the plot can be accurately measured by deploying an additional surface mounted FBG after reaching regime 3 and restricting the use of the initial FBGs measurements to those from regimes 1 through 3.

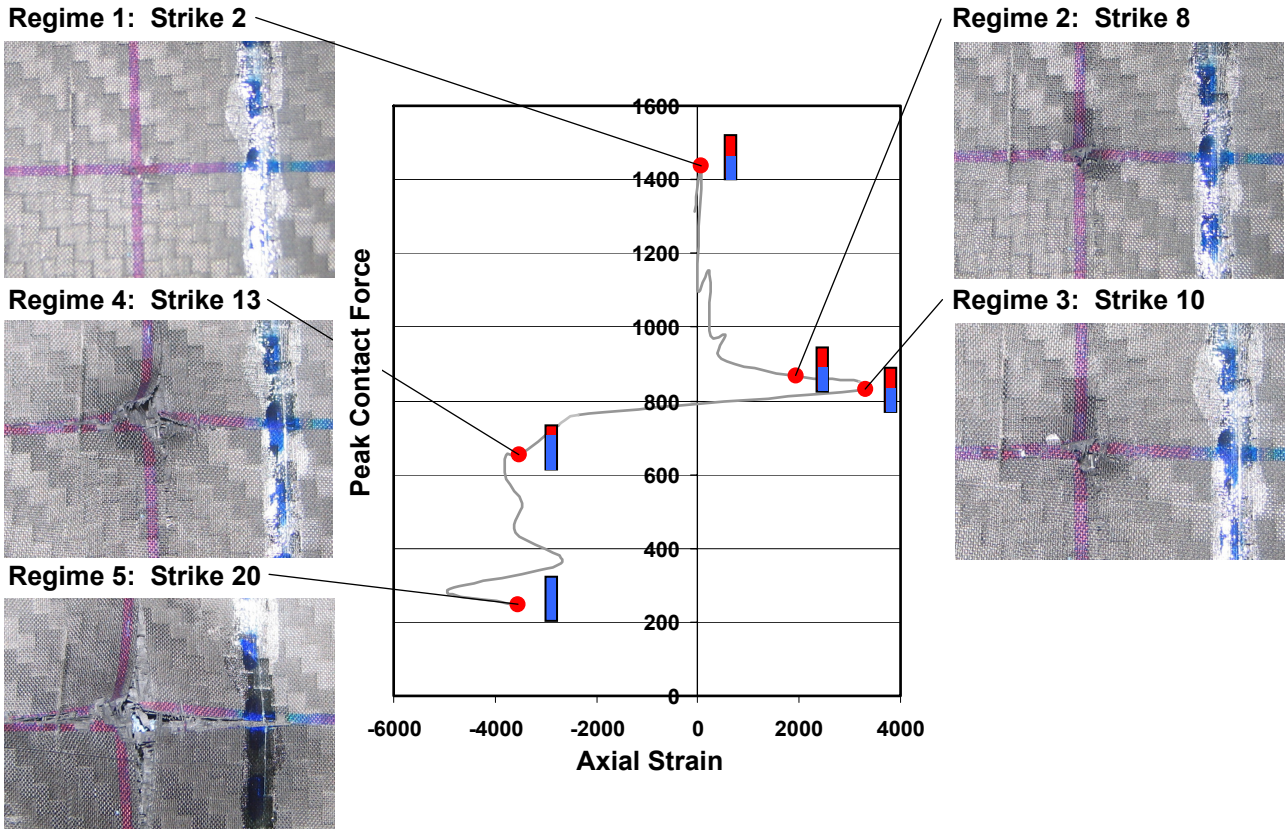

Figure 3: Peak contact force (in N) during impact versus residual axial strain (in με) after impact for each strike of specimen C2. Red data points indicate selected strikes in each regime with visual record of surface deformation after impact. Gray path indicates circuit traced out when all strikes are plotted. Vertical bar at each red point shows average dissipated energy over all strikes within a regime in blue as a fraction of incident kinetic energy in red. As seen in regimes 1 through 3, the fraction of dissipated for all strikes to incident energy is relatively constant at 50% before growing to 75% and 100% in regimes 4 and 5 respectively.

Under certain bonding conditions, such as debonding or a rapidly changing deformation gradient over the gauge length, multiple strain values represented as separate Bragg peaks may be encoded into the FBG spectrum. Instead of a central Bragg peak, regions of the gauge under highly varying strain may be separated into individual Bragg peaks.[23-27] These peaks are not attributable to noise in the spectrum because of their both repeatability and shift, or evolution, in response to additional impacts. Also, these peaks occur before fiber fracture for specimen C2 thus discounting any effect of catastrophic waveguide failure. Furthermore, the separate peaks are not attributable to radiation or cladding modes due to both the lack of any periodic nature in the wavelengths surrounding the main Bragg spectrum and the high relative intensity compared to the background noise.[28]

Multiple strain peaks in a single FBG spectrum are shown in Figure 4. These peaks complicate strain measurement by presenting multiple values, all of which are missed when analyzing the signal through the common, computer friendly centroid method, the result of which is shown with a star.

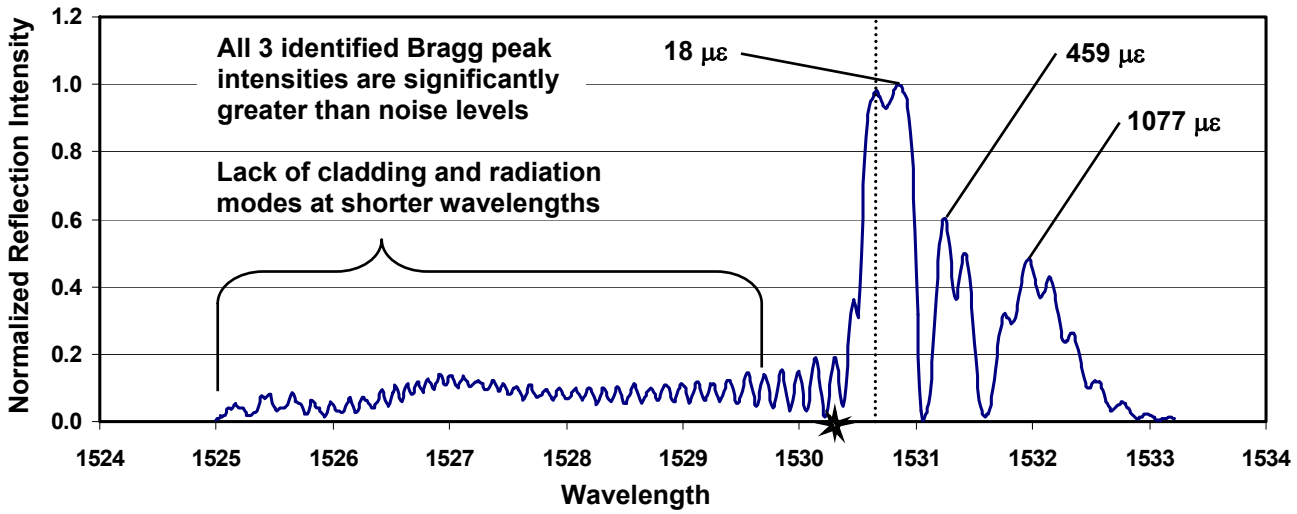

Figure 4: Specimen C2 FBG spectrum after strike 18 as measured from End 2 of the fractured optical fiber in reflection. Three separate, repeatable peaks are identified as well as the indicated strain. Both the Bragg peak calculated by the centroid method (shown with star on the x-axis) and the baseline Bragg wavelength after mounting but before impact (shown by vertical dashed line) are displayed. Note the error and strain peaks missed by the centroid technique under these spectral conditions as well as the lack of cladding modes at shorter wavelengths thus suggesting the multiple strain values are indeed separate Bragg peaks.

To investigate this phenomenon further, Figure 5 plots the strain computed from the FBG mounted on specimen C2 measured from End 1 and End 2 of the fiber respectively. The optical fiber broke at the location of the grating after strike #11. Figures 6 and 7 plot several examples of the measured reflection spectra after selected impact strikes. The progressive widening of the reflected spectrum after strike #4 corresponds to a non-uniform axial strain induced due to impact, as mentioned above. The split in the Bragg peak after strike #8 indicates that one section of the grating is in tension while no strain is applied to the remaining section, an indication of partial sensor debonding. The complex loading occurring due to progression of damage in the composite thus split the single Bragg peak into multiple peaks as the number of strikes progressed. The strains plotted in Figure 5 are computed from the Bragg peaks of the reflection spectrum measured after strikes # 11, 14, 17 and 20 and are indicated on each graph. One observes, as before, that a section of the grating is debonded while the other section is in compression for the section of the grating interrogated from End 1. One observes that sections of the grating are at zero, tensile and compressive strains for the section of the grating interrogated from End 2. Such separate strain regions are typical of impacted or embedded sensors and their discrimination is a unique capability of the FBG strain sensor.[23-27] There is also a change in amplitude of reflection in the two Bragg peaks during the progression of damage. This change in amplitude is due to a changing length of each strained section as the grating splits into multiple sections. The spectra of Figures 6 and 7 are not normalized to demonstrate this reduction in amplitude.

4. CONCLUSIONS

Surface mounted FBG sensors were used to monitor the development of post impact residual strains in woven prepreg composite systems. For specimens with surface mounted sensors, there were five distinct regimes of response with the final two regimes pertaining to the localized debonding and fiber fracture of the FBG. The onset of non-uniform axial strains, which was due to the local discontinuity between individual woven carbon fiber rovings, was detected in regime 2. Continuous post impact interrogation indicated large relaxations in the residual strains occurring over tens of seconds suggesting an additional mode of energy dissipation and storage through internal friction and sliding between delaminated plies. Strain relaxation was found to occur in two modes, a decrease in total axial tension and a relaxation of the axial strain field's non-uniformity. It was also demonstrated that the unique capabilities of the FBG strain sensor provides more accurate interpretation of the developing residual strains. Potential sources of error such as debonding were eliminated from the strain data through the measurement of the complete spectral response of the FBG.

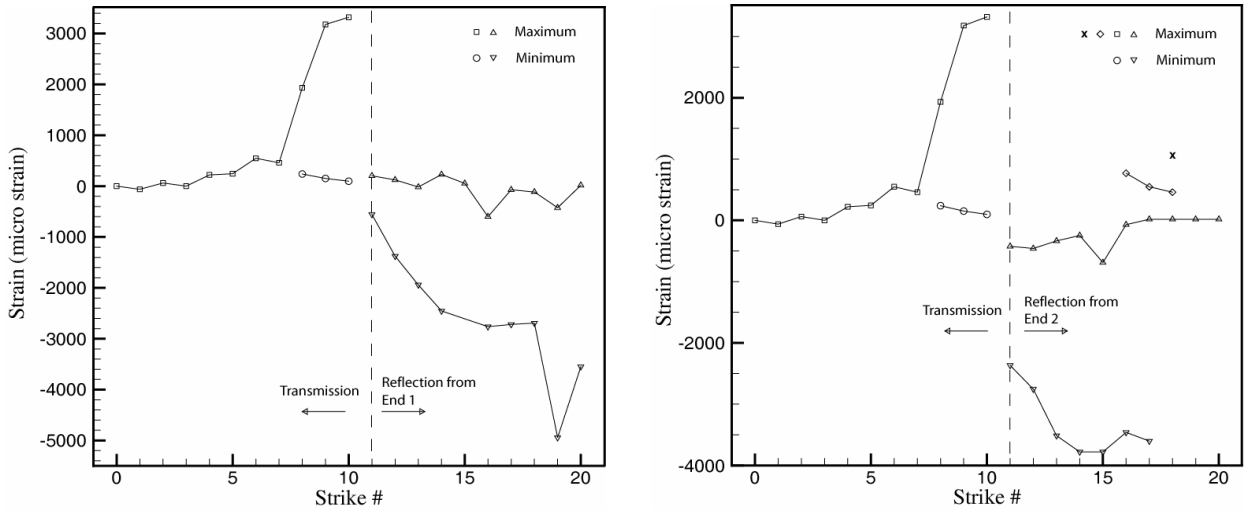

Figure 5: Variation of strain with strike number for FBG mounted on specimen C2. Strains computed from the transmission spectra are plotted before failure of the optical fiber at strike 11. Strains computed from both the reflected spectra of (a) End 1and (b) End 2 are plotted after strike 11.

ACKNOWLEDGEMENTS

The authors gratefully acknowledge the support of the National Science Foundation through grant # CMS 0219690. Furthermore, the authors would like to thank the United Composites Group for donating the woven prepreg stock. The authors would also like to thank Micron Optics for their generous loan of the Si720 Optical Spectrum Analyzer.

REFERENCES

1. Baucom JN, Zikry MA. Evolution of failure mechanisms in 2D and 3D woven composite systems under quasi-static perforation. *Journal of Composite Materials* 2003;Vol. 37 No. 18:1651-1674
2. Friebele E J, Askins C G, et al. Optical fiber sensors for spacecraft applications. *Smart Materials and Structures* 1999;Vol. 8 No. 6:813-838
3. Feraboli Paolo, Masini Attilio. Development of carbon/epoxy structural components for a high performance vehicle. *Composites Part B: Applied Science and Manufacturing* 2004;Vol. 35:323-330
4. Idriss R L, Kodindouma M B, Kersey A D, Davis M A. Multiplexed Bragg grating optical fiber sensors for damage evaluation in highway bridges. *Smart Materials and Structures* 1998;Vol. 7 No. 2:209-216
5. Shah Khan M Z, Grabovac I. Repair of damage to marine sandwich structures: Part II – fatigue testing. Defence Science and Technology Organisation (DSTO) Aeronautical and Maritime Research Laboratory 2000; http://www.dsto.defence.gov.au/corporate/reports/DSTO-TN-0275.pdf
6. Sirkis J S, Lu I-Ping. On interphase modeling for optical fiber systems embedded in unidirectional composite systems. *Journal of Intelligent Material Systems and Structures* 1995;Vol. 6:199-209
7. Betz D C, Staudigel L, Trutzel M N, Kehlenback M. Structural monitoring using fiber-optic Bragg grating sensors. *Structural Health Monitoring* 2003;Vol. 2 No. 2:145-152
8. Betz D C, Staudigel L, Trutzel M N. Test of a fiber Bragg grating sensor network for commercial aircraft structures. *Optical Fiber Sensors Conference Technical Digest, 2002, 15th International Conference on Optical Fiber Sensors, Portland USA*;Vol. 1:55-58
9. Ecke W, Latka I, Willsch R, Reutlinger A, Graue R. Fibre optic sensor network for spacecraft health monitoring. *Measurement Science and Technology* 2001;Vol. 12:974-980
10. Murukeshan V M, Chan P Y, Ong L S, Seah L K. Cure monitoring of smart composites using fiber Bragg grating based embedded sensors. *Sensors and Actuators A: Physical* 2000;Vol. 79 Issue 2:153-161

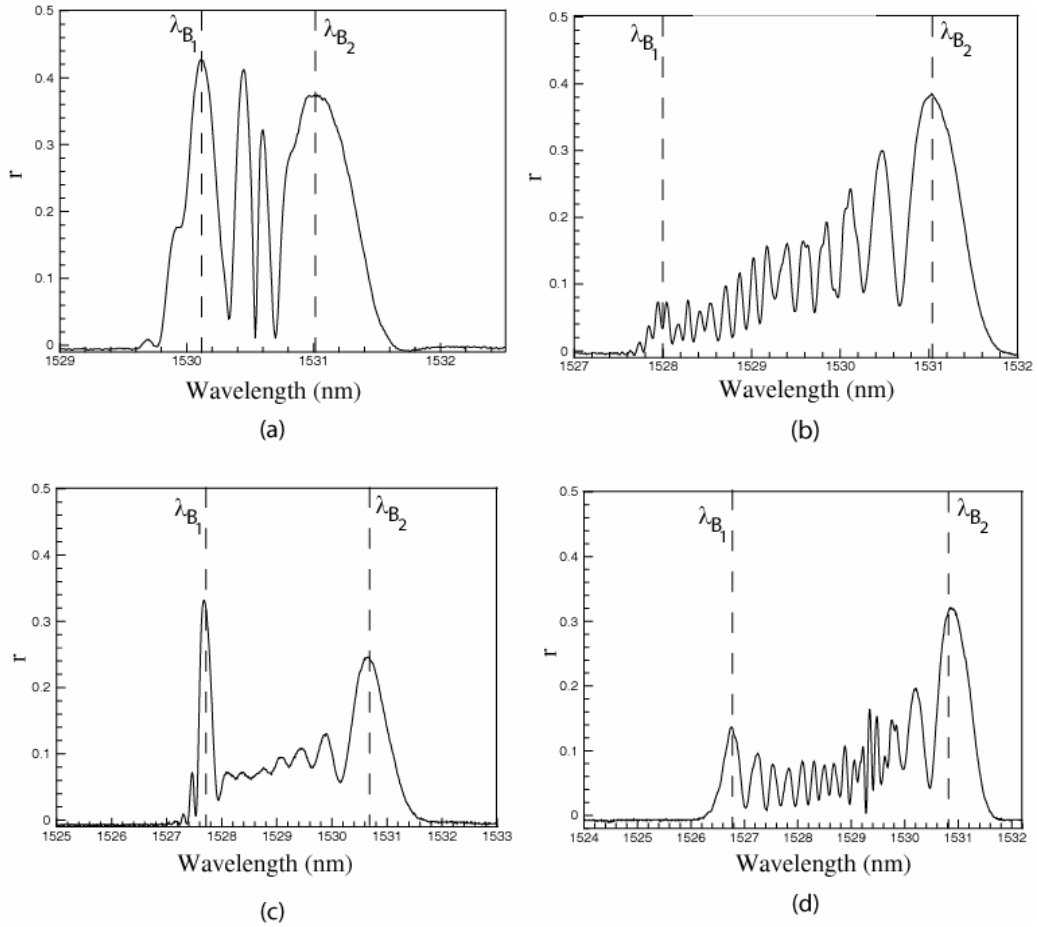

Figure 6: Measured reflection spectra from End 1 for FBG surface mounted on specimen C2 after strikes number: (a) 11, (b) 14, (c) 17 and (d) 20.

11. Leng J S, Asundi A. Real-time cure monitoring of smart composite materials using extrinsic Fabry-Perot interferometer and fiber Bragg grating sensors. *Smart Materials and Structures* 2002;Vol. 11 No. 2:249-255
12. Doyle C, Martin A, Liu T, Wu M, Hayes S, Crosby P A, Powell G R, Brooks D, Fernando G F. In-Situ process and condition monitoring of advanced fiber-reinforced composite materials using optical fibre sensors. *Smart Materials and Structures* 1998;Vol. 7 No. 2:145-158
13. Giordano M, Laudati A, Nasser J, Nicolais L, Cusano A, Cutolo A. Monitoring by a single fiber Bragg grating of the process induced chemo-physical transformations of a model thermoset. *Sensors and Actuators A: Physical* 2004;Vol. 113 Issue 2:166-173
14. Bocherens E, Bourasseau S, Dewynter-Marty V, Py S, Dupont M, Ferdinand P, Berenger H. Damage detection in a radome sandwich material with embedded fiber optic sensors. *Smart Materials and Structures* 2000;Vol. 9 No. 3:310-315
15. Bayandor J, Thomson R S, Scott M L, Nquyen M Q, Elder D J. Investigation of impact and damage tolerance in advanced aerospace composite structures. *International Journal of Crashworthiness* 2003;Vol. 8 No. 3:297-306
16. Güemes J A, Menendez J M, Frövel M, Fernandez I, Pintado J M. Experimental analysis of buckling in aircraft skin panels by fibre optic sensors. *Smart Materials and Structures* 2001;Vol. 10 No. 3:490-496

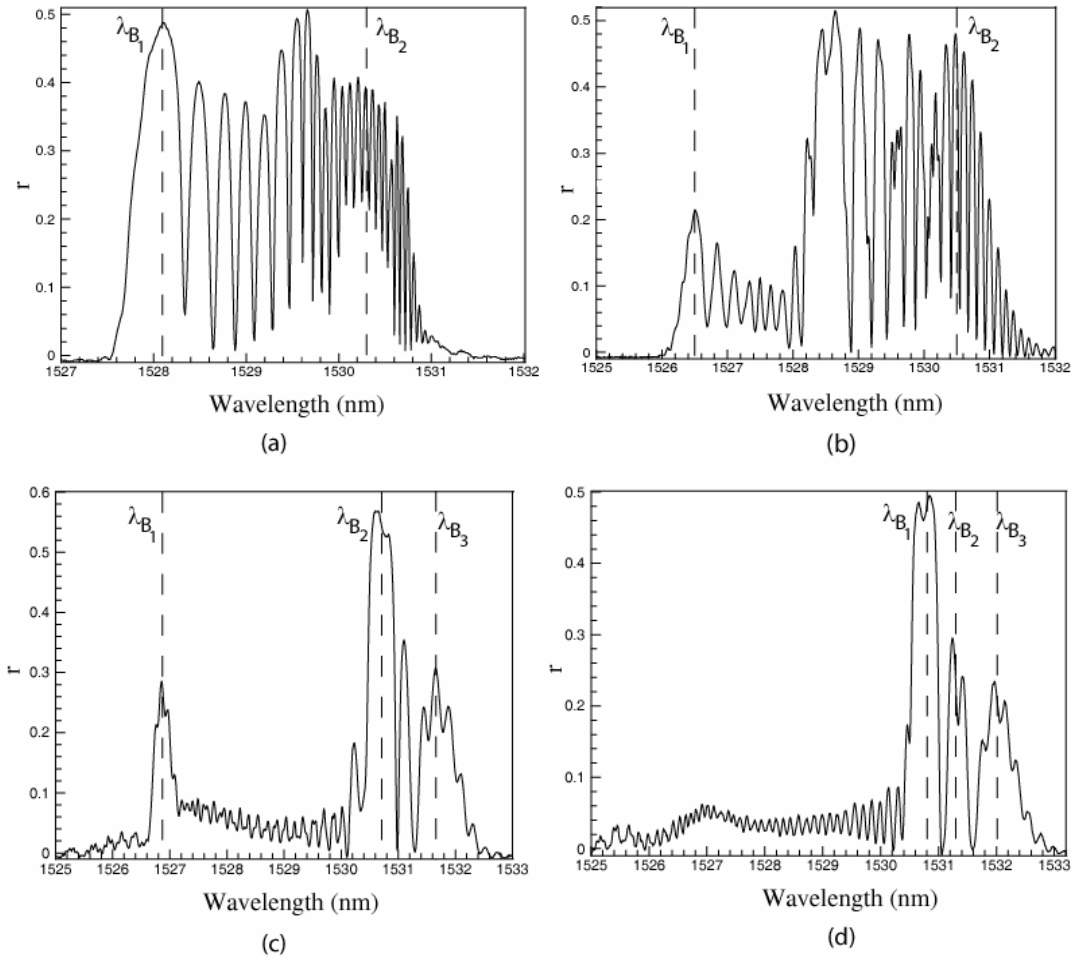

Figure 7: Measured reflection spectra from End 2 for FBG surface mounted on specimen C2 after strikes number: (a) 11, (b) 14, (c) 16 and (d) 18.

17. Waele W De, Degrieck J, Moerman W, Taerwe L, Baets P De. Feasibility of integrated optical fibre sensors for condition monitoring of composite structures Part 1: Comparison of Bragg-sensors and strain gauges. *INSIGHT – Non-Destructive Testing and Condition Monitoring* April 2003;Vol. 45 No. 4:266-271
18. Yang B, Tao X M, Yu J, Ho H L. Compression force measured by fiber optic smart cellular textile composites. *Textiles Research Journal* 2004;Vol. 74 No. 4:305-313
19. Fernando G F, Webb D J, Ferdinand P. Optical-fiber sensors. *MRS Bulletin* 2002;Vol. 27 No. 5:359-361
20. Davies G A O, Zhang X. Impact Damage prediction in carbon composite structures. *International Journal of Impact Engineering* 1994;Vol. 16 No. 1:149-170
21. Belingardi G, Vadori R. Low velocity impact tests of laminates glass-fiber-epoxy matrix composite material plates. *International Journal of Impact Engineering* 2002;Vol. 27:213-229
22. Shyr Tien-Wei, Pan Yu-Hao. Impact resistance and damage characteristics of composite laminates. *Composite Structures* 2003;Vol. 62:193-203
23. Kuang K S C, Kenny R, Whelan, M P, Cantwell W J, Chalker P R. Embedded fibre Bragg grating sensor in advance composite materials. *Composites Science and Technology* 2001;Vol. 61:1379-1387.
24. Guemes J A, Menendez J M. Reponse of Bragg grating fiber-optic sensors when embedded in composite laminates. *Composites Science and Technology* 2002;Vol. 62:959-966.
25. Okabe Y, Yashiro S, Kosaka T, Takeda N. Detection of transverse cracks in CFRP composites using embedded fiber Bragg grating sensors. *Smart Materials and Structures* 2000;Vol. 9:832-838.

26. Kuang K S C, Kenny R, Whelan, M P, Cantwell W J, Chalker P R. Residual strain measurement and impact response of optical fibre Bragg grating sensors in fibre metal laminates. *Smart Materials and Structures* 2001;Vol.10:338-346.
27. Studer M, Peters K, Botsis J. Method for determination of crack bridging parameters using long optical fiber Bragg grating sensors. *Composites Part B* 2003;Vol. 34:347-359.
28. Erdogan T. Cladding-mode resonances in shot- and long-period fiber gratings filters. *Journal of the Optical Society of America A* 1997;Vol. 14:1760-1773